Hindawi Publishing Corporation
International Journal of Photoenergy
Volume 2012, Article ID 356943, 11 pages
doi:10.1155/2012/356943

Research Article

Photoelectrochemical Performance of Smooth TiO_2 Nanotube Arrays: Effect of Anodization Temperature and Cleaning Methods

Chin Wei Lai and Srimala Sreekantan

School of Materials and Mineral Resources Engineering, Universiti Sains Malaysia, Engineering Campus, Seberang Perai Selatan, Pulau Pinang, 14300 Nibong Tebal, Malaysia

Correspondence should be addressed to Srimala Sreekantan, srimala@eng.usm.my

Received 9 December 2011; Revised 20 February 2012; Accepted 20 February 2012

Academic Editor: James T. Mcleskey

The formation of self-organized titanium dioxide (TiO_2) nanotube arrays without bundling or clustering is essential for their high efficiency in photoelectrochemical (PEC) application. The present paper reports on the use of different temperatures to control the specific architecture of nanotube arrays and effective cleaning techniques to ensure the formation of clean TiO_2 nanotube surface. The wall thickness of nanotube arrays could be controlled from 12.5 nm to 37.5 nm through different anodization temperature ranging from 10°C to 80°C. Furthermore, ultrasonic cleaning combined with acetone showed the high-ordered TiO_2 nanotube arrays without morphological disorder, bundling, and microcrack problems. Based on the results obtained, a higher PEC response of 1 mA/cm^2 and a photoconversion efficiency of 1.3% could be achieved using a wall thickness of 12.5 nm and defect-free TiO_2 nanotube arrays for low charge transfer resistance.

1. Introduction

At present, modern society is habituated to a high degree of mobility, fast communication, and daily comfort, all of which require considerable energy input. The increase in world population and industrial development has all led to accelerated energy consumption, which, in turn, leads to various diseases and global warming [1]. Due to these factors, new energy sources that are inexhaustible and nonpolluting have been studied intensively [2–4]. In recent years, interest in photocatalysts for the production of hydrogen as a clean fuel, as concerns over the cost of fossil fuels to the economy, environment, and national security have become paramount. In these aspects, one-dimensional titanium dioxide (TiO_2) has emerged as the leading candidate for developing hydrogen fuel cell as a potential future energy and possibly the best substitute for fossil fuel [5, 6]. The uniform morphology, better charge transfer properties, and high surface area with controllable pore size of TiO_2 nanotube arrays make them a promising functional material in photoelectrochemical (PEC) application [7–12]. However, the ability to produce the best dimension for such application has remained a major challenge.

Geometrical features of the nanotube arrays, including length, pore diameter, and wall thickness, are controlled by a variety of parameters, such as anodic voltage, anodization time, electrolyte composition (fluoride content, viscosity, and pH), electrolyte temperature, and surface condition of nanotube arrays [13–15]. However, a detailed investigation on the effect of electrolyte temperature and effective cleaning technique to produce clean TiO_2 nanotube arrays for PEC performance is lacking. Electrolyte temperature plays a critical role in the determination of the final dimensions of the nanotubes' various surface morphologies and architectures [12, 16]. The earlier report on the effect of electrolyte temperature has been reported by Mor et al. since 2005 [17]. They reported that wall thickness of the nanotube was increased with decreasing anodization temperature while the length of the nanotube increases with decreasing anodization bath temperature from 50°C to 5°C. Later, Wang and lin claimed that the diameters of nanotube arrays are smaller in an ice bath condition when anodized in organic electrolyte

[18]. However, their anodization process was only conducted either at room temperature or in an ice bath. Next, Chen et al. reported that the inner diameter of the tubes increases with increasing electrolyte temperature from 10°C to 35°C. They found that the tube profile could be improved from the general V-shape to a U-shape by gradually increasing the electrolyte temperature [19]. However, the listed work was conducted at low electrolyte temperature; details on the investigation using higher temperature (>50°C) were not reported. The present paper studies the electrochemical anodization of Ti foil in organic electrolyte (ethylene glycol (EG)), with main focus on the effect of electrolyte temperatures from 10°C to 80°C on the growth of TiO_2 nanotube arrays.

Previous researchers have studied various cleaning procedures for TiO_2 nanotubes and have come up with an effective way of producing clean TiO_2 nanotube surfaces. Zhu et al. reported that TiO_2 nanotube arrays cleaned with ethanol, followed by the supercritical CO_2 drying technique, could effectively remove the structural disorder from oriented TiO_2 nanotube arrays by removing capillary stress [20]. Later, Kim et al. claimed that the structural disorder (nanograss) and bundling problem of TiO_2 nanotube arrays could be avoided by forming a protective top layer on polished Ti samples to delay the chemical attack of the tube ends [21]. However, these techniques are costly and complicated. In addition, some authors have reported that hydrofluoric acid (HF) treatment can significantly remove the precipitated layer on the top surface of nanotubes [18, 22–24]. However, the issue is still far from being solved. The chemical etching of HF for as-anodized TiO_2 nanotubes can remove the precipitated layer, but etching the nanotube surface can make it serrated and irregular in texture [18, 24]. The serrated surface and nanotube disorder could significantly retard PEC performance due to the higher density of surface recombination in the photoinduced electrons [20]. To minimize the distortion-induced surface defects in nanotube arrays and reduce the consumption of hazardous chemical from HF, the present study introduces a simple, cost-effective, fast, and environmentally safe technique for producing highly specific clean surface areas of TiO_2 nanotube arrays using ultrasonic cleaning combined with acetone. The high aspect ratio, bundle-free TiO_2 nanotube arrays alter the spatial dimensionality of the transport and recombination mechanism, which affect photon absorption efficiency and PEC response [12, 15, 20, 25]. The mechanistic understanding of various electrolyte temperatures and cleaning methods is very important for the controlled growth of ordered TiO_2 nanotube structures, which have potential uses in the development of viable hydrogen fuel cell for a sustainable energy system.

2. Experimental

A total of 99.6% Ti foils, with a thickness of 0.127 mm (STREM Chemicals), were used in the current study. Ti foils were cut into desired dimensions (50 mm × 10 mm). Before anodization, the Ti foils were degreased in ethanol through sonication for 30 min. The foils were then rinsed in deionized (DI) water and dried by the blowing of nitrogen. After drying, the Ti foil was placed in 100 mL EG containing 5 wt% ammonium fluoride (NH_4F) and 5 wt% hydrogen peroxide (H_2O_2) [15]. Anodization was performed in a two-electrode bath with Ti foil as the anode and a platinum rod as the cathode. The experiments were conducted at 10°C to 80°C electrolyte temperature.

During the anodization process, air bubble was blown in the electrolyte to maintain a uniform current near the Ti foil. Anodization was done at a constant potential of 60 V using a Keithley DC Power Supply for 1 h. After the anodization process, as-anodized Ti foils were cleaned using different cleaning treatments. For the first approach, ultrasonic cleaning combined with DI water was applied to the as-anodized sample using a WiseClean Ultrasonic Cleaner WUC-A06H (40 kHz, 150 W). For the second approach, the as-anodized sample was cleaned using DI water with a hot rinse at 90°C. For the third approach, ultrasonic cleaning combined with 2% HF was applied to the as-anodized sample. The last approach used ultrasonic cleaning combined with acetone for the as-anodized sample. All samples were dried in nitrogen stream. After the cleaning and drying treatments, the as-anodized samples were annealed at 400°C for 4 h in argon atmosphere for conversion into the TiO_2 anatase phase. The morphology of the anodized Ti foils was viewed using a field emission scanning electron microscope (FESEM) (Zeiss SUPRA 35VP) at a working distance of approximately 1 mm. To obtain the thickness of the anodic oxide formed, cross-sectional measurements were conducted on mechanically bent samples, wherein a partial lift-off of the anodic layer occurred. Phase determination of the anodic layer was determined via XRD (Philips, PW 1729), operated at 45 kV and 40 mV. The Raman spectra were recorded at room temperature using an LS 55 luminescence spectrometer (Jobin-Yvon HR 800UV).

The PEC properties of the samples were characterized using a three-electrode PEC cell, with TiO_2 nanotube arrays as the working photoelectrode, platinum rod as a counterelectrode, and saturated calomel electrode (SCE) as the reference electrode. A solution of 1 M KOH with 1 wt% EG was used as the electrolyte in the current experiment. All three electrodes were connected to the potentiostat (μAutolab III), and the current and voltage were measured. An 800 W/m^2 xenon lamp (Zolix LSP-X150) was used to produce a largely continuous and uniform spectrum; the quartz glass permitted 100% transmittance of the light as the xenon lamp shined on the TiO_2 nanotube arrays (photoanode). The xenon lamp was switched on after the three electrodes were connected to the potentiostat. During the voltage sweeping (5 mV/s), the corresponding photocurrent was measured. Subsequently, the photocurrent was plotted against the potential applied. The photoconversion efficiency (η) for the water splitting reaction was calculated based on the following equation [26–28]:

$$\eta\ (\%) = j_p \frac{[(V_{ws} - V_B)]}{I_o}, \quad (1)$$

where j_p is the photocurrent density (mA/cm^2); V_{ws} is 1.229 V is the potential corresponding t the Gibbs free energy

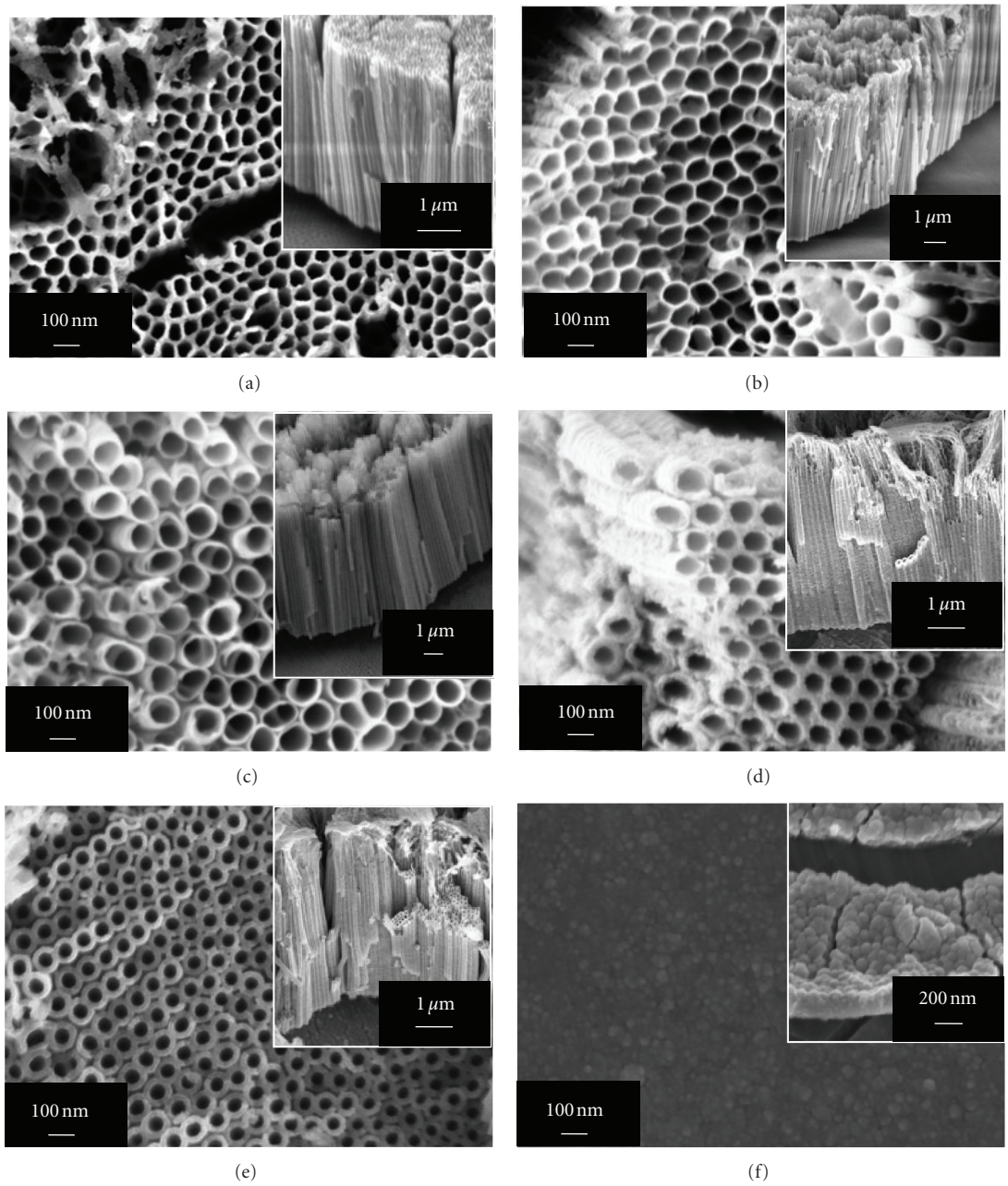

Figure 1: FESEM images of TiO_2 nanotube arrays fabricated at (a) 10°C, (b) 20°C, (c) room temperature, (d) 40°C, (e) 60°C, and (f) 80°C in ethylene glycol electrolyte containing 5 wt% H_2O_2 and 5 wt% NH_4F anodized at 60 V for 1 h. Insets are the cross-section morphologies of the TiO_2 nanotube arrays.

change per photon required to split water; V_B is the bias voltage applied between the working and counterelectrodes; I_o is the power density of the incident light (mW/cm^2).

3. Results and Discussion

3.1. Effect of Anodization Temperature. The current section discusses the effect of anodization temperature on the morphology of the TiO_2 array nanotubes. Figure 1 shows the FESEM images of the surface morphology of the Ti foils anodized in EG containing 5 wt% H_2O_2 and 5 wt% NH_4F at 60 V for 1 h with various anodization temperatures ranging from 10°C to 80°C. Insets are the cross-section morphologies of the TiO_2 nanotube arrays. These images show that the appearance of anodic oxides on the Ti foils was dependent on the anodization temperature in the fluorinated electrolyte. The relationship of the length, pore diameter, and wall thickness of the tubes with different anodization temperatures are summarized in Figure 2(a). In this graph, two different stages are shown to indicate the changing dimensions of TiO_2

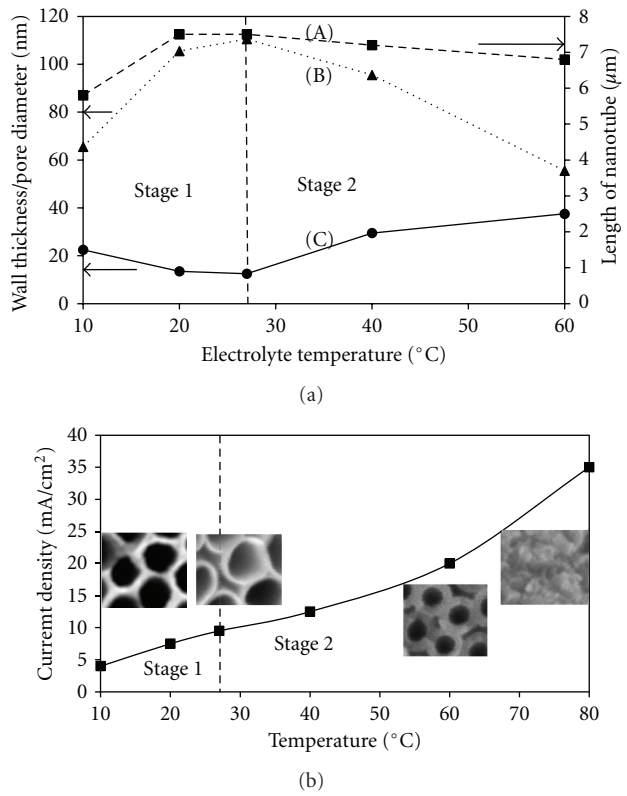

Figure 2: (a) Effect of anodization temperature on the (A) length, (B) pore diameter, and (C) wall thickness of the TiO_2 nanotube arrays anodized at 60 V for 1 h; (b) current density as function of anodization temperature.

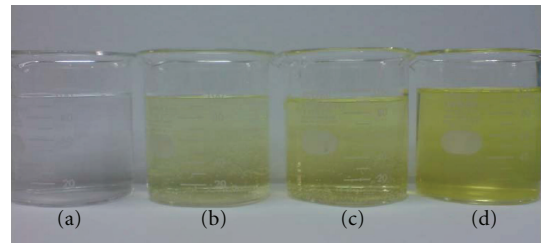

Figure 3: Color of electrolyte obtained upon Ti foil anodized in ethylene glycol containing NH_4F and H_2O_2 (a) before anodization process, (b) at 10°C, (c) at room temperature, and (d) at 60°C.

nanotube arrays at various electrolyte temperatures. Stage 1 represents the cool condition of the electrolyte, which was below room temperature (27°C), whereas Stage 2 represents the warm condition of the electrolyte, which was beyond room temperature (27°C).

The sample anodized at a low temperature of 10°C (Figure 1(a)) produced nanotubes with an inner pore diameter of ~65.5 nm, a length of ~5.8 μm, and a wall thickness of ~22.5 nm. The FESEM image shows microcracks or defects in this sample. When the anodization temperature was increased to 20°C, the inner pore diameter of the nanotubes increased to an average 105.5 nm, and the length to ~7.5 μm; however, the wall thickness decreased to ~13.5 nm (Figure 1(b)). The shape of the nanotubes became much more uniform, compared with those produced at low anodization temperatures. When the anodization process was subsequently conducted at room temperature (27°C), TiO_2 nanotube arrays exhibited an average inner pore diameter of 110.5 nm, a length of ~7.5 μm, and a wall thickness of 12.5 nm (Figure 1(c)). Smooth, circular nanotube arrays were obtained at room temperature without a defect in the large area. When the electrolyte temperature was increased to 40°C, the wall thickness of the nanotube increased to 29.5 nm, with an inner pore diameter of 95.5 nm, and a length of approximately 7.2 μm (Figure 1(d)). Further increasing the temperature to 60°C increased the wall thickness of the nanotubes to 37.5 nm, with an inner pore diameter of 55.5 nm, and a length of approximately 6.8 μm (Figure 1(e)). However, further increasing the electrolyte temperature to 80°C negatively affected the self-organization of the anodic oxide, wherein the nanotube structure disappeared and anodic oxide consisted of an irregular porous layer, as shown in Figure 1(f). The thickness of the porous layer was approximately 0.3 μm.

In Stage 1, a temperature of up to 27°C reduced the tube's wall thickness and increased its length. The difference in wall thickness may be attributed to the increasing current density with temperature. This result clearly indicates that the chemical dissolution is increased, as shown in Stage 1 in Figure 2(b). At this stage, the rate of the oxide dissolution reaction is believed to be faster than that of Ti etching. This assumption may be attributed to the higher driving force for ionic transport through the barrier layer at higher temperatures that cause fast movements of the F^- and H^+ species at the Ti/TiO_2 interface, thus resulting in the formation of thin nanotube walls [12, 16, 19].

In Stage 2, the wall thickness of the tube structure significantly increased. Furthermore, higher current density was found in the case of higher temperature environment (Figure 2(b)). This result may be attributed to the excessive Ti^{4+} ions diffusing outward and the O^{2-} ions transported inward at a faster rate under high temperature oxidation environments, which resulted in the formation of thick-walled TiO_2 nanotube arrays. This statement is further supported by the interaction between excessive Ti^{4+} ions with H_2O_2 that resulted in the intense yellowish color of electrolyte at higher temperature (Figure 3(d)), compared with the pale yellowish electrolyte at a lower temperature (Figure 3(b)) [29]. However, beyond 80°C of the electrolyte is detrimental to the formation of self-organized nanotube arrays. The chemical etching exceeded anodic oxidation, and the balance required for self-ordering was diminished. The results of the current study indicate that the growth of nanotube arrays is due to the competition between field-assisted oxide dissolution and the diffusion rate of ionic species, field-assisted oxidation of Ti, and the chemical etching process that could be controlled by the anodization temperature. Thus, the equilibrium reactions are important in driving the Ti/TiO_2 interface deeper into the Ti foil. A schematic illustration of the diffusion rate of ionic species

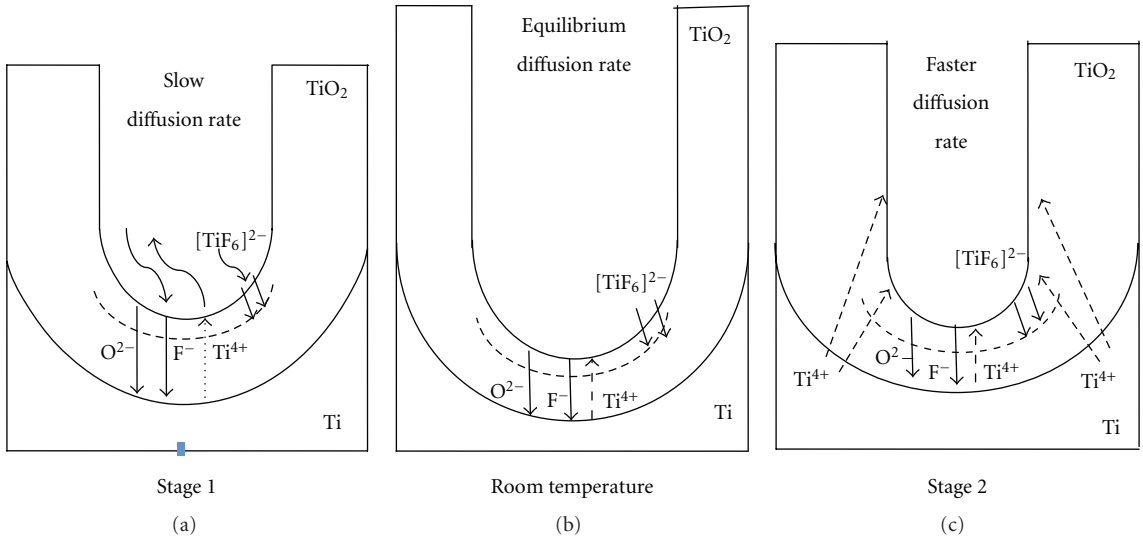

Figure 4: Schematic illustration explaining the diffusion rate of ionic species at metal-oxide layers above the Ti foil, (a) Stage 1 (cool condition), (b) room temperature (27°C), and (c) Stage 2 (warm condition).

at the barrier layer at different temperatures is exhibited in Figure 4.

The crystal structure of the as-anodized and TiO_2 nanotubes after annealing at 400°C in argon atmosphere fabricated at various electrolyte temperatures were identified via XRD. As-anodized TiO_2 nanotubes with an amorphous structure and no crystalline phase were observed at 10°C to 80°C anodization temperature (Figure 5(a)). The only peaks related to the Ti substrate were exhibited. These results indicate that the anodization temperature is not sufficient to induce the crystallinity of TiO_2. Therefore, heat treatment was conducted at 400°C, and TiO_2 nanotubes were found to be crystalline with anatase TiO_2. As shown in the XRD patterns in Figure 5(b), the peaks from anatase TiO_2 can be detected at 2θ of 25.5°, 38.5°, 48°, 54.5°, and 55.5°, which correspond to (101), (004), (200), (105), and (211), respectively. Although, the predominant anatase phases were detected in all samples, the peak intensities of (101) at 25.5°, (004) at 38.5°, (200) at 48°, (105) at 54.5°, and (211) at 55.5° for the sample fabricated at room temperature, 40°C, and 60°C were stronger than the sample produced at 10, 20, and 80°C. This result implies that higher thickness of the nanotube layer is responsible for the higher intensity of the anatase peaks (Figure 5 versus Figure 2). This is evident from the reduction in Ti peak intensities.

To verify the results, selected samples were analyzed via Raman to validate the crystal structure and presence of the anatase phase (Figure 6). The as-anodized TiO_2 nanotube arrays fabricated at 40 and 60°C were affirmed to be amorphous in nature; no anatase peak was observed in the Raman spectrum. However, a major band position at 192, 390, 510, and 635 cm^{-1} was detected in the annealed TiO_2 nanotubes, corresponding to the bonding vibration of anatase phase. All samples formed anatase as the dominant phase after the annealing process at 400°C in argon atmosphere.

3.2. Effect of Different Cleaning Methods after Anodization. After the anodization process, TiO_2 nanotubes are often covered with precipitates that need to be removed using suitable cleaning agents and methods. The pores on the oxide layer are formed because of the fluoride ions and the electric field-assisted dissolution. Both oxidation and chemical dissolutions are active at the bottom of the pores. In this condition, Ti^{4+} was dissolved and ejected from the nanopore to the surface, and accumulated at the entrance of the nanopore. This phenomenon could be the $Ti(OH)_4$ formed via the instantaneous hydrolysis reaction, which leads to the generation and accumulation of $Ti(OH)_4$ precipitate at the entrance of the nanopores to form the flaky structure on the surface TiO_2 nanotube [12, 30]. Therefore, the type of solvent and technique required in removing the solvent from the tubular structure is critical. This phenomenon is discussed in detail in the following section.

For comparison, a set of experiments was conducted in EG with the addition of 5 wt% H_2O and 5 wt% NH_4F under the same anodization conditions. All samples were anodized at 60 V for 1 h at room temperature. One of the samples was ultrasonically cleaned in distilled water for 1 min and subsequently dried under flowing N_2 gas. Figure 7(a) shows the top and side view images of the as-anodized sample before annealing. The image clearly shows the presence of clusters of nanotube bundles and microcrack formation. Such structure is believed to be caused by the capillary stress created during the evaporation of liquids from the nanotubes [20]. The unbalanced capillary stress within the interior and exterior of the pores accelerates the distortion of the pore structure near the ends of the nanotube, collapsing to produce an overlayer that covers the opening of the nanotubes. The extent of unbalanced capillary stress is dependent on the nanotube length and the surface tension of the cleaning solvent. A similar observation

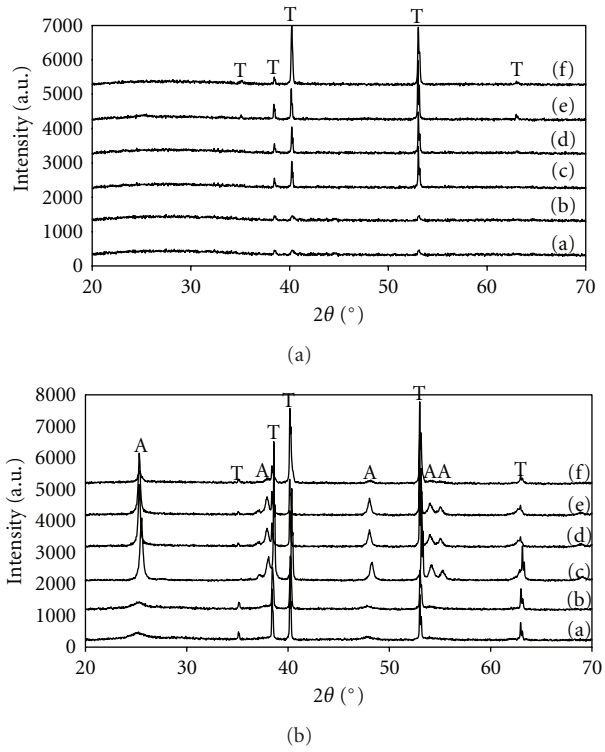

Figure 5: (a) XRD patterns of as-anodized TiO_2 nanotube arrays fabricated at (a) 10°C, (b) 20°C, (c) room temperature, (d) 40°C, (e) 60°C, and (f) 80°C; (b) XRD patterns of annealed TiO_2 nanotube arrays fabricated at (a) 10°C, (b) 20°C, (c) room temperature, (d) 40°C, (e) 60°C, and (f) 80°C after annealing at 400°C in argon atmosphere (A: anatase TiO_2; T: titanium).

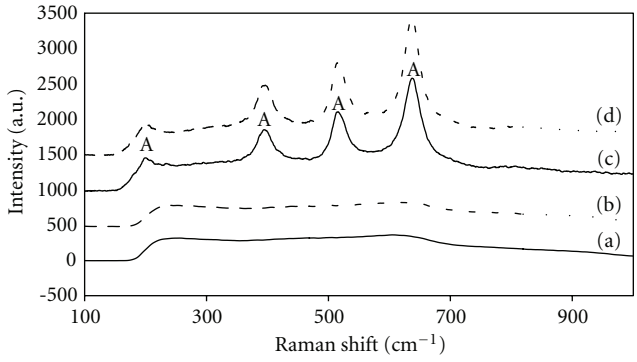

Figure 6: Raman spectra of (a) as-anodized TiO_2 nanotube arrays fabricated at 40°C, (b) as-anodized TiO_2 nanotube arrays fabricated at 60°C, (c) annealed TiO_2 nanotube arrays fabricated at 40°C, and (d) annealed TiO_2 nanotube arrays fabricated at 60°C (A: anatase).

was found in the sample cleaned by hot rinsing at 90°C using distilled water for 1 min and subsequently dried under flowing N_2 gas (Figure 7(b)). The presence of clusters of TiO_2 nanotube bundles and microcracks were evident in the sample.

The samples fabricated under the same conditions were cleaned via two different approaches: (1) chemical etching using 2% HF with ultrasonic and (2) ultrasonic cleaning using acetone. Figure 8 shows the FESEM images of as-anodized nanotubes ultrasonically cleaned with 2% HF for 10, 15, 20, and 60 s. The apparent overlayers still covered the end of the nanotube channels. The different cleaning times had no significant effect on the top view of the nanotubes. However, the length of the nanotubes was reduced from 7.5 μm to 6.0 μm after 20 s (Figure 8(c)), and the length was further reduced to 3.5 μm after 60 s (Figure 8(d)). A longer cleaning time in HF might have increased the etching rate. Consequently, the nanotubes tend to break and collapse on each other, thus forming overlayers that cover them.

Figure 9 shows the FESEM images of TiO_2 nanotubes cleaned with acetone, followed by 1, 2, and 10 min of ultrasonic agitation under condition of 150 W and 40 kHz. The overlayer that covered the nanotube was minimized through ultrasonic agitation for 1 and 2 min (Figures 9(a) and 9(b)). These results show a better result of self-standing, well-ordered nanotubes with a clear opening. The nanotube arrays have an average length of 7.5 μm and a diameter of approximately 90 nm. Figure 9(c) shows the FESEM images for 10 min of ultrasonic agitation. The nanotube length was shorter by 4 μm. This result could be because the TiO_2 wall could not sustain the agitation for a longer period; thus, the nanotubes broke down to form shorter nanotubes. The broken nanotubes led to overlayer formation that covered the short nanotubes. Based on the result obtained, approximately 1 or 2 min ultrasonic agitation in acetone is effective in removing overlayers from the nanotubes leading to the formation of free-standing TiO_2 nanotube arrays without breaking the tube structure. This result is in agreement with the work reported by Xu et al. [31], in which they reported that treating time of ultrasonic was extended to 40 min, nanotubes broke down to form shorter tubes and no nanotubes were left on the Ti substrate if the treating time of ultrasonic further increased to 60 min.

The working principle of ultrasonic cleaning is performed using sound waves to microscopically scrub and clean all internal and external surfaces of the nanotube in the presence of acetone. The higher frequency of ultrasonic cleaning, combined with acetone, can penetrate deeper and clean away the $Ti(OH)_4$ precipitate layer at the entrance of the nanotube arrays. During ultrasonic cleaning, numerous gas bubbles are formed. The great amount of pressure exerted on the gas bubble leads to a sudden cavitation implosion. Thus, the liquid molecules collide, releasing a vast amount of energy that rapidly increases local temperature, producing a high-energy liquid stream that collides with the surface of the nanotube arrays. The reasons can be attributed to the cavitations, acoustic streaming, strong agitation and thermal oscillating flow initiated by the ultrasonic vibration that eventually increase the local temperature and produce a high energy liquid stream. This theoretical has been reported by Oh et al. and Feng et al. [32, 33]. Thus, the collision agitates contaminants adhering to the surface of the nanotube, which effectively and efficiently dislodges them at micron levels.

Another reason for the reduced degree of morphological disorder in ultrasonic agitation combined with acetone could be attributed to lower surface tension. This result indicates that acetone can reduce the surface tension and capillary

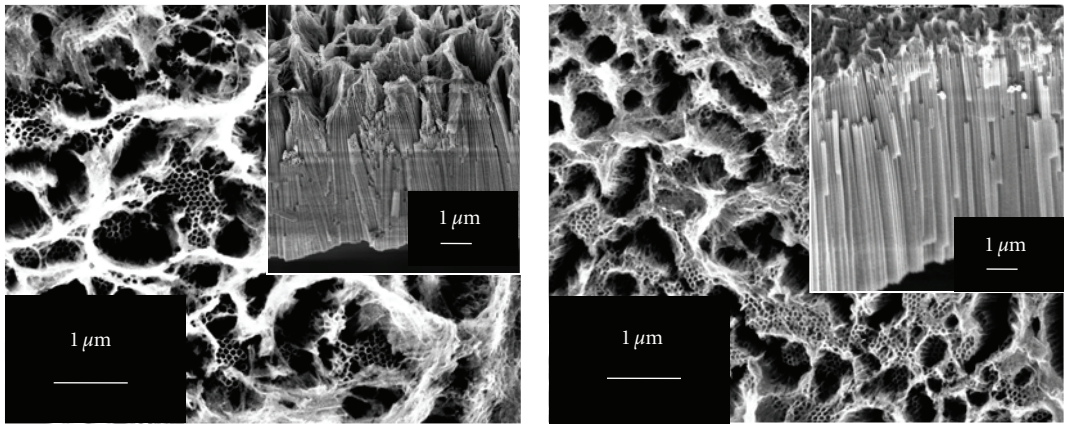

(a) (b)

Figure 7: FESEM images of TiO_2 nanotubes obtained via different cleaning methods after the anodization process; (a) ultrasonically cleaned in distilled water for 1 min and subsequently dried under flowing N_2 gas and (b) cleaned by hot rinsing at 90°C using distilled water for 1 min and subsequently dried under flowing N_2 gas.

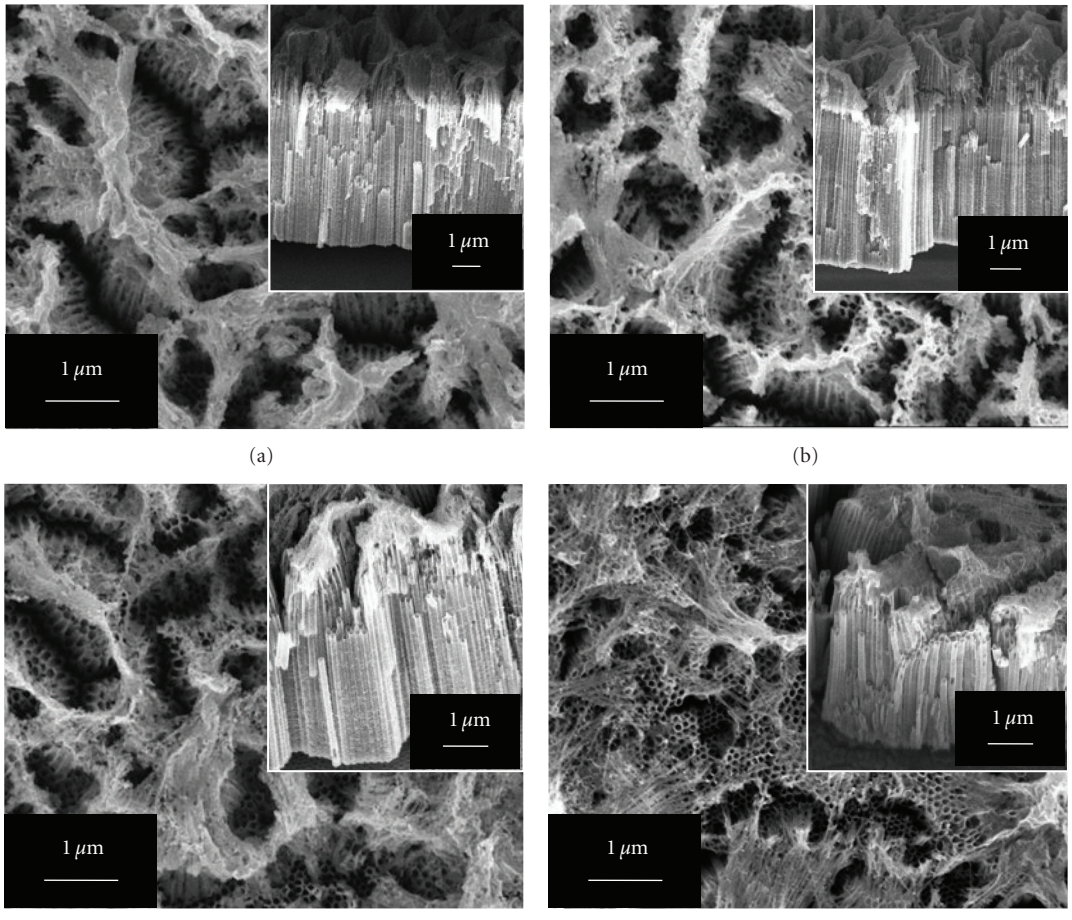

(a) (b)

(c) (d)

Figure 8: FESEM images of TiO_2 nanotubes obtained via chemical etching using 2% HF after anodization for (a) 10, (b) 15, (c) 20, and (d) 60 s.

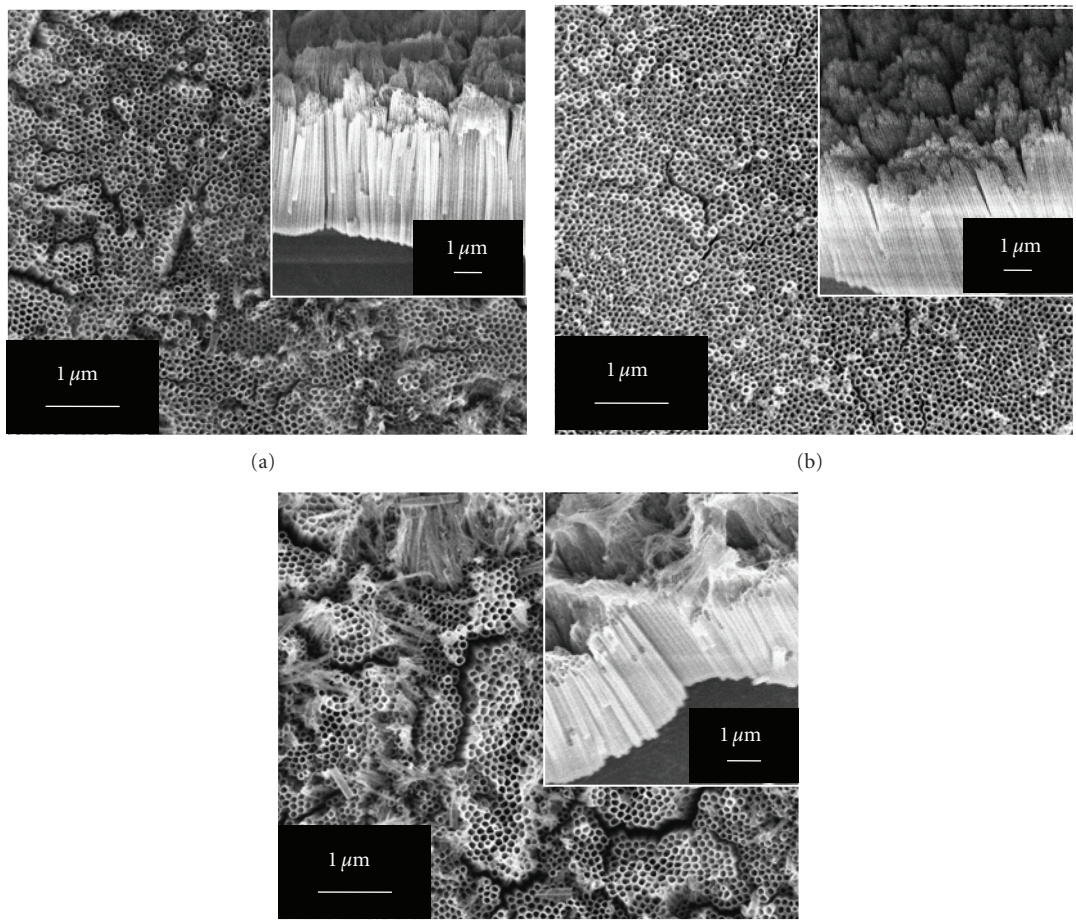

Figure 9: FESEM images of TiO_2 nanotubes obtained via ultrasonic cleaning using acetone after anodization for (a) 1, (b) 2, and (c) 10 min.

stress between the adjacent nanotube arrays, resulting in bundle-free and crack-free TiO_2 nanotube arrays as compared with the sample cleaned in distilled water. Acetone is a fast-evaporating cleaning detergent solution with lower surface tension and an inherent cleaning property, which results in the superior microcleaning of the nanotube surface.

3.3. PEC Response on TiO_2 Nanotube Fabricated at Different Anodization Temperatures. The variation of photocurrent responses as a function of applied potentials (*I-V* characteristics) for TiO_2 fabricated at different anodization temperatures was evaluated under illumination, as shown in Figure 10. Based on the previous part of the experiment, anodization temperature significantly affects the tube length, pore diameter, and wall thickness of nanotubes. The high-ordered TiO_2 nanotube arrays without morphological disorder, bundling, and microcrack problems can significantly enhance the transport properties and reduce the recombination of charge carriers (e^-/h^+), which extends the residence time of electrons [20]. Therefore, studying the different surface morphologies of clean TiO_2 nanotubes under different anodization temperatures on the PEC response is very important.

The initial chemical potential of electrons in a semiconductor and an electrolyte is determined through the Fermi energy of the semiconductor and the redox potential of the redox couples in the electrolyte, respectively. When a TiO_2 photoanode is submerged in the electrolyte, the initial chemical potential of the electrons is different for the two phases. Charge redistribution between TiO_2 and solution is required to equilibrate the two phases; hence, a space charge layer (depletion layer) will form in the TiO_2 adjacent to the electrolyte. For tube-shaped *n*-type TiO_2 semiconductor, majority of the photoinduced charge carriers (e^-/h^+) are generated at both sides of the tube walls and the entire tube sidewalls, which consist of space charge layers. Theoretically, the space charge layer is necessarily close to the tube wall to generate the photocurrent under illumination [25, 34]. The photoinduced electrons in this space charge layer transfer from the TiO_2 nanotubes photoanode will migrate towards the bulk of the TiO_2 and eventually these photoinduced electrons move to counterelectrode (Pt) with an external bias, while the photoinduced holes move to the electrolyte under illumination. This situation will cause the valence and conduction bands to move relatively to the Fermi level (bend upwards) by an illumination of energy greater than the

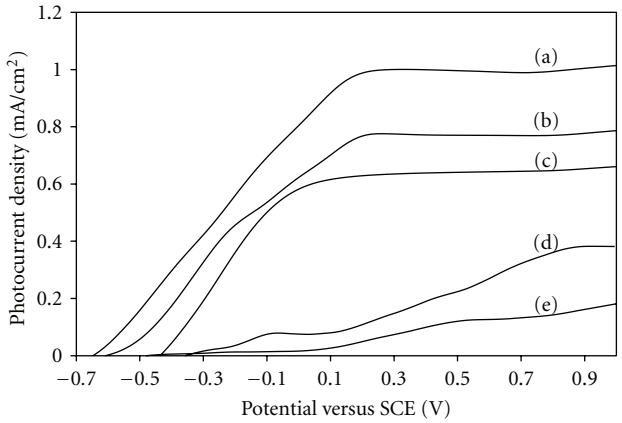

Figure 10: I-V characteristics of TiO_2 nanotubes under light-on condition at (a) room temperature, (b) 40, (c) 60, (d) 10, and (e) 80°C anodization temperatures.

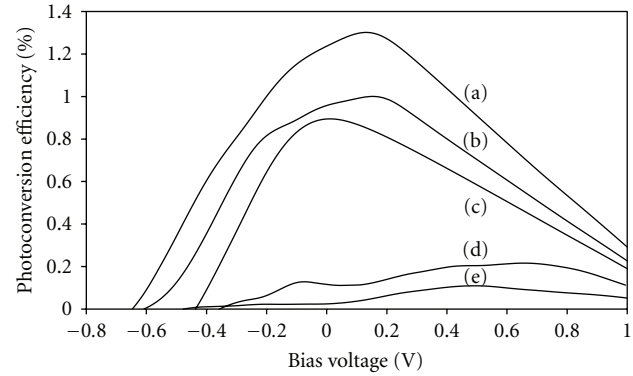

Figure 11: Corresponding photoconversion efficiencies of TiO_2 nanotubes at (a) room temperature, (b) 40, (c) 60, (d) 10, and (e) 80°C anodization temperatures.

band gap of TiO_2 nanotubes photoanode [35]. In this case, an electric field will be generated and, therefore, potential barriers will form along the inner and outer surfaces of the nanotubes [25, 34–37].

The current density was approximately 10^{-7}A to 10^{-6} A in the dark condition for the entire sample. However, the photocurrent density increased under illumination. Therefore, TiO_2 nanotubes can act well as a representative n-type semiconductors for the transfer and decay of the photoinduced electrons under light pulse illumination. The wall thickness of the sample fabricated at room temperature showed the highest photocurrent density throughout the potential window. This result suggests an efficient charge separation. The photocurrent reached a high value of 1 mA/cm^2, whereas samples fabricated at 40, 60, 10, and 80°C showed a decreased photocurrent density of approximately 0.7, 0.6, 0.3, and 0.1 mA/cm^2, respectively. The highest photocurrent density, 1 mA/cm^2, indicates that the width of space charge layer is near to the wall thickness of the nanotube (~12.5 nm). Therefore, this sample effectively generates more photoinduced electrons transfer to the counterelectrode and has a great tendency to reduce the recombination of charge carriers (e^-/h^+). However, samples with thicker tube walls produced at 40 and 60°C exhibited poor photocurrent density. This result indicates that wall thickness is significantly larger than the width of the space charge layer, which may be attributed to the transfers of photoinduced electrons to the counterelectrode (Pt) and the photoinduced holes to the surface of TiO_2 nanotubes photoanode were hindered due to the longer path to cross and these charge carriers will recombine readily. Thus, poor PEC performance exhibited due to the less of photoinduced electrons for reduction reaction and less of photoinduced holes for the oxidation of electrolyte species. In addition, the length of the nanotube is another important factor in controlling its PEC performance. Poor photoresponses were recorded for the short TiO_2 nanotubes (5.8 μm) produced at 10°C, which have an irregular TiO_2 oxide layer with a thickness of 0.3 μm. Shorter nanotubes and oxide layers have less effective surface areas for light (photon) absorption, which definitely limits the chemical reactions that allow the photocurrent to generate [38–40]. In summary, these results clearly imply that wall thickness and nanotube length play important roles in enhancing the migration of photoinduced electrons to the counterelectrode (Pt) through external circuit for reduction reaction and thus influence PEC performance.

The photoconversion efficiency (η) for the water splitting reaction was calculated based on the two-electrode configuration. The main reason is because of the applied bias voltage is versus the counterelectrode and not the reference electrode. Thus, the second half-reaction of water splitting process occurring at the counterelectrode is included in the two electrode configuration photoconversion efficiency [26, 27]. Figure 11 shows that the maximum photoconversion efficiency is obtained from the sample produced at room temperature was 1.3%, followed by the photoconversion efficiency of 1.1%, 0.9%, 0.2%, and 0.1% obtained at 40, 60, 10, and 80°C anodization temperatures, respectively. Such differences in photocurrent and photoconversion efficiencies reflect the overall photoelectron efficiency in generation, separation, and transport for the sample fabricated in different anodization temperatures with different surface morphologies.

4. Conclusion

Self-organized TiO_2 nanotube arrays were successfully synthesized from a low temperature of 10°C to a high temperature of 60°C in EG electrolyte containing 5 wt% NH_4F and 5 wt% H_2O_2 at 60 V for 1 h. Nanoporous TiO_2 favors temperatures beyond 80°C. Based on the result obtained, anodization temperature significantly affects the wall thickness, length, and pore size. The length of the tubes decreased, whereas its wall thickness increased when synthesized at low and high temperatures. Furthermore, approximately 1 or 2 min of ultrasonic agitation in acetone is effective in removing overlayers on the nanotubes. This process results in the formation of bundle-free and crack-free TiO_2 nanotube arrays. In addition, the thin wall and higher length of the

TiO_2 nanotube arrays fabricated at room temperature exhibit the highest photocurrent density at 1 mA/cm^2, with a maximum photoconversion efficiency of 1.3%. This result is due to the effective transfer of photoinduced electrons to the counterelectrode (Pt) with an external bias, which has a great tendency to reduce the recombination of charge carriers (e^-/h^+) at the thin walls of the nanotubes.

Acknowledgments

The author would like to thank Universiti Sains Malaysia for sponsoring this work under RU grant 814075, PRGS grant 8044058, FRGS grant 6071213, Fellowship USM and Research University Postgraduate Research Grant Scheme, 80430146.

References

[1] M. Kitano, M. Matsuoka, M. Ueshima, and M. Anpo, "Recent developments in titanium oxide-based photocatalysts," *Applied Catalysis A*, vol. 325, no. 1, pp. 1–14, 2007.

[2] M. Grätzel, "Dye-sensitized solar cells," *Journal of Photochemistry and Photobiology C*, vol. 4, no. 2, pp. 145–153, 2003.

[3] V. M. Aroutiounian, V. M. Arakelyan, and G. E. Shahnazaryan, "Metal oxide photoelectrodes for hydrogen generation using solar radiation-driven water splitting," *Solar Energy*, vol. 78, no. 5, pp. 581–590, 2005.

[4] E. Y. Kim, J. H. Park, and G. Y. Han, "Design of TiO_2 nanotube array-based water-splitting reactor for hydrogen generation," *Journal of Power Sources*, vol. 184, no. 1, pp. 284–287, 2008.

[5] G.-J. Wang, G.-Y. Chen, and M.-W. Lee, "Fabrication of dye-sensitized solar cells with a 3D nanostructured electrode," *International Journal of Photoenergy*, vol. 2010, Article ID 585621, 7 pages, 2010.

[6] S. K. Mohapatra, M. Misra, V. K. Mahajan, and K. S. Raja, "A novel method for the synthesis of titania nanotubes using sonoelectrochemical method and its application for photoelectrochemical splitting of water," *Journal of Catalysis*, vol. 246, no. 2, pp. 362–369, 2007.

[7] S.-J. Kim, N.-H. Lee, H.-J. Oh, S.-C. Jung, W.-J. Lee, and D.-H. Kim, "Photocatalytic properties of nanotubular-shaped TiO_2 powders with anatase phase obtained from titanate nanotube powder through various thermal treatments," *International Journal of Photoenergy*, vol. 2011, Article ID 327821, 7 pages, 2011.

[8] S. Kim, S. J. Hwang, and W. Choi, "Visible light active platinum-ion-doped TiO_2 photocatalyst," *Journal of Physical Chemistry B*, vol. 109, no. 51, pp. 24260–24267, 2005.

[9] M. Paulose, H. E. Prakasam, O. K. Varghese et al., "TiO_2 nanotube arrays of 1000 μm length by anodization of titanium foil: Phenol red diffusion," *Journal of Physical Chemistry C*, vol. 111, no. 41, pp. 14992–14997, 2007.

[10] M. Anpo and M. Takeuchi, "The design and development of highly reactive titanium oxide photocatalysts operating under visible light irradiation," *Journal of Catalysis*, vol. 216, no. 1-2, pp. 505–516, 2003.

[11] M. Ni, M. K. H. Leung, D. Y. C. Leung, and K. Sumathy, "A review and recent developments in photocatalytic water-splitting using TiO_2 for hydrogen production," *Renewable and Sustainable Energy Reviews*, vol. 11, no. 3, pp. 401–425, 2007.

[12] D. Wang, Y. Liu, B. Yu, F. Zhou, and W. Liu, "TiO_2 nanotubes with tunable morphology, diameter, and length: synthesis and photo-electrical/catalytic performance," *Chemistry of Materials*, vol. 21, no. 7, pp. 1198–1206, 2009.

[13] C. Trapalis, N. Todorova, T. Giannakopoulou, G. Romanos, T. Vaimakis, and J. Yu, "Preparation of fluorine-doped TiO_2 photocatalysts with controlled crystalline structure," *International Journal of Photoenergy*, vol. 2008, Article ID 534038, 9 pages, 2008.

[14] K. Yasuda, J. M. MacAk, S. Berger, A. Ghicov, and P. Schmuki, "Mechanistic aspects of the self-organization process for oxide nanotube formation on valve metals," *Journal of the Electrochemical Society*, vol. 154, no. 9, pp. C472–C478, 2007.

[15] S. Sreekantan, L. C. Wei, and Z. Lockman, "Extremely fast growth rate of TiO_2 nanotube arrays in electrochemical bath containing H_2O_2," *Journal of the Electrochemical Society*, vol. 158, no. 12, pp. C397–C402, 2011.

[16] J. M. Macak and P. Schmuki, "Anodic growth of self-organized anodic TiO_2 nanotubes in viscous electrolytes," *Electrochimica Acta*, vol. 52, no. 3, pp. 1258–1264, 2006.

[17] G. K. Mor, K. Shankar, M. Paulose, O. K. Varghese, and C. A. Grimes, "Enhanced photocleavage of water using titania nanotube arrays," *Nano Letters*, vol. 5, no. 1, pp. 191–195, 2005.

[18] J. Wang and Z. Lin, "Anodic formation of ordered TiO_2 nanotube arrays: effects of electrolyte temperature and anodization potential," *Journal of Physical Chemistry C*, vol. 113, no. 10, pp. 4026–4030, 2009.

[19] X. Chen, J. Chen, and J. Lin, "Self-assembled TiO_2 nanotube arrays with U-shaped profile by controlling anodization temperature," *Journal of Nanomaterials*, vol. 2010, Article ID 753253, 4 pages, 2010.

[20] K. Zhu, T. B. Vinzant, N. R. Neale, and A. J. Frank, "Removing structural disorder from oriented TiO_2 nanotube arrays: reducing the dimensionality of transport and recombination in dye-sensitized solar cells," *Nano Letters*, vol. 7, no. 12, pp. 3739–3746, 2007.

[21] D. Kim, A. Ghicov, and P. Schmuki, "TiO_2 Nanotube arrays: elimination of disordered top layers ("nanograss") for improved photoconversion efficiency in dye-sensitized solar cells," *Electrochemistry Communications*, vol. 10, no. 12, pp. 1835–1838, 2008.

[22] G. K. Mor, M. A. Carvalho, O. K. Varghese, M. V. Pishko, and C. A. Grimes, "A room-temperature TiO_2-nanotube hydrogen sensor able to self-clean photoactively from environmental contamination," *Journal of Materials Research*, vol. 19, no. 2, pp. 628–634, 2004.

[23] Y. Liu, J. Li, B. Zhou et al., "Comparison of photoelectrochemical properties of TiO_2-nanotube- array photoanode prepared by anodization in different electrolyte," *Environmental Chemistry Letters*, vol. 7, no. 4, pp. 363–368, 2009.

[24] K. Kant and D. Losic, "A simple approach for synthesis of TiO_2 nanotubes with through-hole morphology," *Physica Status Solidi—Rapid Research Letters*, vol. 3, no. 5, pp. 139–141, 2009.

[25] L. Sun, S. Zhang, X. Sun, and X. He, "Effect of the geometry of the anodized titania nanotube array on the performance of dye-sensitized solar cells," *Journal of Nanoscience and Nanotechnology*, vol. 10, no. 7, pp. 4551–4561, 2010.

[26] A. B. Murphy, P. R. F. Barnes, L. K. Randeniya et al., "Efficiency of solar water splitting using semiconductor electrodes," *International Journal of Hydrogen Energy*, vol. 31, no. 14, pp. 1999–2017, 2006.

[27] Z. Chen, T. F. Jaramillo, T. G. Deutsch et al., "Accelerating materials development for photoelectrochemical hydrogen production: standards for methods, definitions, and reporting protocols," *Journal of Materials Research*, vol. 25, no. 1, pp. 3–16, 2010.

[28] K. Shankar, G. K. Mor, M. Paulose, O. K. Varghese, and C. A. Grimes, "Effect of device geometry on the performance of TiO_2 nanotube array-organic semiconductor double heterojunction solar cells," *Journal of Non-Crystalline Solids*, vol. 354, no. 19–25, pp. 2767–2771, 2008.

[29] N. K. Allam, K. Shankar, and C. A. Grimes, "Photoelectrochemical and water photoelectrolysis properties of ordered TiO_2 nanotubes fabricated by Ti anodization in fluoride-free HCl electrolytes," *Journal of Materials Chemistry*, vol. 18, no. 20, pp. 2341–2348, 2008.

[30] S. Li, G. Zhang, D. Guo, L. Yu, and W. Zhang, "Anodization fabrication of highly ordered TiO_2 nanotubes," *Journal of Physical Chemistry C*, vol. 113, no. 29, pp. 12759–12765, 2009.

[31] H. Xu, Q. Zhang, C. Zheng, W. Yan, and W. Chu, "Application of ultrasonic wave to clean the surface of the TiO_2 nanotubes prepared by the electrochemical anodization," *Applied Surface Science*, vol. 257, no. 20, pp. 8478–8480, 2011.

[32] Y. K. Oh, S. H. Park, and Y. I. Cho, "A study of the effect of ultrasonic vibrations on phase-change heat transfer," *International Journal of Heat and Mass Transfer*, vol. 45, no. 23, pp. 4631–4641, 2002.

[33] H. Feng, G. Barbosa-Canovas, and J. Weiss, *Ultrasound Technologies for Food and Bioprocessing*, Springer, Berlin, Germany, 2011.

[34] A. Ghicov and P. Schmuki, "Self-ordering electrochemistry: a review on growth and functionality of TiO_2 nanotubes and other self-aligned MO_x structures," *Chemical Communications*, no. 20, pp. 2791–2808, 2009.

[35] M. Grätzel, "Photoelectrochemical cells," *Nature*, vol. 414, no. 6861, pp. 338–344, 2001.

[36] C. A. Grimes, "Synthesis and application of highly ordered arrays of TiO_2 nanotubes," *Journal of Materials Chemistry*, vol. 17, no. 15, pp. 1451–1457, 2007.

[37] Y. Xie, L. Zhou, and J. Lu, "Photoelectrochemical behavior of titania nanotube array grown on nanocrystalline titanium," *Journal of Materials Science*, vol. 44, no. 11, pp. 2907–2915, 2009.

[38] S. Yeonmi and L. Seonghoon, "Self-organized regular arrays of anodic TiO_2 nanotubes," *Nano Letters*, vol. 8, no. 10, pp. 3171–3173, 2008.

[39] C. W. Lai and S. Sreekantan, "Effect of applied potential on the formation of self-organized TiO_2 nanotube arrays and its photoelectrochemical response," *Journal of Nanomaterials*, vol. 2011, Article ID 142463, 7 pages, 2011.

[40] M. Paulose, G. K. Mor, O. K. Varghese, K. Shankar, and C. A. Grimes, "Visible light photoelectrochemical and water-photoelectrolysis properties of titania nanotube arrays," *Journal of Photochemistry and Photobiology A*, vol. 178, no. 1, pp. 8–15, 2006.